Solution Structures and Integrin Binding Activities of an RGD Peptide with Two Isomers†

Nuria Assa-Munt,* Xin Jia, Pirjo Laakkonen, and Erkki Ruoslahti*

Cancer Research Center, The Burnham Institute, 10901 North Torrey Pines Road, La Jolla, California 92037

Received September 6, 2000; Revised Manuscript Received December 5, 2000

ABSTRACT: The Arg-Gly-Asp (RGD) sequence serves as the primary integrin recognition site in extracellular matrix proteins, and peptides containing this sequence can mimic the activities of the matrix proteins. Depending on the context of the RGD sequence, an RGD-containing peptide may bind to all of the RGD-directed integrins, to a few, or to only a single one. We have previously isolated from a phage-displayed peptide library a cyclic peptide that binds avidly to the $\alpha_v\beta_3$ and $\alpha_v\beta_5$ integrins but does not bind to other closely related integrins. This peptide, ACDCRGDCFCG, exists in two natural configurations depending on internal disulfide bonding. The peptide with the 1−4; 2−3 disulfide bond arrangement accounts for most of the α_v integrin binding activity, whereas the 1−3; 2−4 peptide is about 10-fold less potent. Solution structure analysis by nuclear magnetic resonance reveals an entirely different presentation of the RGD motif in the two isomers of RGD-4C. These results provide new insight into the ligand recognition specificity of integrins.

Integrins are the main cell surface receptors mediating cell adhesion to extracellular matrices (*1*, *2*). Integrins are heterodimers of an α subunit and a *β* subunit, and each *αβ* combination has its individual ligand binding specificity. Some 25 integrins are known, and at least eight of them bind to the Arg-Gly-Asp (RGD)[1] motif as the primary recognition sequence in their ligands. Peptides that have little secondary structure bind to all of these integrins, whereas conformational restriction of the RGD sequence in a peptide, combined with an appropriate choice of the amino acids that flank the RGD, can yield more specific peptides. These conformationally restricted peptides can bind specifically to one RGD-directed integrin only or to a small group of closely related integrins (*2*, *3*).

Peptides that are specific for individual integrins are of considerable interest and medical significance. RGD peptides and peptidomimetics that block the activity of the platelet integrin $\alpha_{IIb}\beta_3$ without interfering with other integrins are already in clinical use. RGD peptides that specifically block the $\alpha_v\beta_3$ integrin show promise as inhibitors of tumor angiogenesis (*4*), retinal angiogenesis (*5*), and osteoporosis (*6*) and in targeting drugs (*7*) into tumor vasculature.

The ACDCRGDCFCG (RGD-4C) peptide we have analyzed here is one of the peptides with promising integrin specificity. Originally isolated from a phage-displayed peptide library by screening on the $\alpha_v\beta_5$ integrin, RGD-4C was shown to be a potent binder (affinity constant of ∼100 nM) of the $\alpha_v\beta_5$ and $\alpha_v\beta_3$ integrins. Both of these integrins are selectively expressed in angiogenic vasculature (*4*, *5*, *8*, *9*). The RGD-4C peptide does not bind appreciably to RGD-directed integrins $\alpha_5\beta_1$, $\alpha_v\beta_1$, and $\alpha_{IIb}\beta_3$ (*10*). Indeed, phage carrying this peptide home specifically to tumor vasculature, and anticancer drugs coupled to the peptide are more active and less toxic against human breast cancer xenograft tumors in nude mice than unmodified drugs (*7*, *11*, *12*). Moreover, investigators have grafted RGD peptides, including RGD-4C, to surface proteins of adenoviruses to change the infectivity pattern of the virus from all human cells to those expressing RGD-directed integrins (*13*, *14*). Such viral vectors, if specific for $\alpha_v\beta_3$, could be particularly useful in gene therapy.

Given the importance of the $\alpha_v\beta_3$ and $\alpha_v\beta_5$ integrins and the peptides that bind to them, we analyzed the binding specificity and solution structure of the RGD-4C peptide. Because of its four cysteine residues, this peptide has three possible fully disulfide-bonded forms. We have found that only two of these forms are present in detectable quantities in the spontaneously cyclized peptide: the one in which the disulfide bridges span the first (Cys_1) and fourth (Cys_4) and the second (Cys_2) and third (Cys_3) cysteine residues (1−4; 2−3) and the one with the 1−3; 2−4 arrangement. We report here that the 1-4; 2-3 form (RGD-A) is a far stronger binder of the $\alpha_v\beta_3$ integrin than the 1−3; 2−4 (RGD-B) form and that the structures for these isomers as determined by nuclear magnetic resonance (NMR) analysis are quite different.

MATERIALS AND METHODS

Peptide Synthesis. The ACDCRGDCFCG peptide was synthesized to our specifications by AnaSpec (San Jose, CA). We have denoted the cysteine positions in the peptide (C_2,

† This work was supported by Grants CaP CURE (N.A.-M.) and CA28896 and CA74238 (E.R.) and Cancer Center Support Grant CA30199 from the National Cancer Institute. P.L. was supported by a fellowship from the Academy of Finland.

* To whom correspondence should be addressed. Phone: (858) 646-3100. E-mail: nuria@burnham.org and ruoslahti@burnham.org.

[1] Abbreviations: RGD, Arg-Gly-Asp; NMR, nuclear magnetic resonance; Acm, acetamidomethyl; HPLC, high-performance liquid chromatography; NOESY, nuclear Overhauser effect spectroscopy; TOCSY, total correlation spectroscopy; DQF-COSY, double-quantum-filtered correlation spectroscopy; HMQC, heteronuclear multiple-quantum experiments; GRASP, graphical representation and analysis of structural properties; TPPI, time-proportional phase incrementation; rmsd, rms deviation.

10.1021/bi002101f CCC: $20.00
Published on Web 02/02/2001

C_4, C_8, and C_{10}) as Cys1, Cys2, Cys3, and Cys4 following their order of appearance in the peptide. To simplify the nomenclature of the disulfide bridges, these were further abbreviated to 1, 2, 3, and 4, respectively, so a bridge from Cys1 to Cys4 and from Cys2 to Cys3 is denoted 1−4 and 2−3, respectively, etc. To synthesize specifically the two isomers with the 1−4; 2−3 and 1−3; 2−4 disulfide bond arrangement, two of the cysteines were blocked with the acetamidomethyl (Acm) protecting group. After cyclization through the unprotected cysteines, the Acm groups were removed with iodine in acetic acid, and the remaining disulfide bond formed in an additional cyclization step. HPLC purification was performed at AnaSpec using an HP model 1090 instrument and a C-18 Rainin column, 86-200-C5. The peptides were eluted using a gradient of A (100% water in 0.1 M TFA) and B (100% acetontrile in 0.1 M TFA) with a flow rate of 1 mL/min. The peptides were extremely pure (>90%). MALDI-TOF mass spectrometry analysis was performed on each disulfide-bridged peptide. The theoretical mass expected for the 1−3; 2−4 peptide was 1146.3, and the experimentally obtained value was 1145.7. For the 1−4; 2−3 doubly disulfide bridged peptide, a theoretical mass of 1145.3 was calculated and the experimental mass was 1145.2. The detection limit for the MASS spectrometer is 0.1. Each peptide eluted as a single peak via high-performance liquid chromatography (HPLC) and displayed the expected mass number in mass spectrometry. The two isomers, once formed, were stable over several months in the chosen DMSO solvent as shown by repeated analysis by NMR. The RGD-4C peptide was also synthesized without directing the disulfide bond formation. As determined by NMR analysis, the ratio of the two isomers (the third theoretically possible conformer, 1−2; 3−4, was not detected) varied from 50:50 to a 90:10 predominance of the 1−4; 2−3 form for the spontaneously cyclized peptide. Various control peptides were synthesized following standard procedures.

Antibodies. The function-blocking antibodies, anti-$\alpha_v\beta_3$ MAB1976, anti-α_4 D49d (clone P1H4) MAB16983Z, anti-β_1 MAB1965, and anti-β_2 MAB1388Z, were from Chemicon (Temecula, CA). Anti-CD11b/Mac1, MO31962, was from Pharmingen (San Diego, CA).

Phage Binding Assay. The attachment of phage to cells was quantitated by incubating 10^{10} transducing units (TU) of phage for 90 min with $1-2 \times 10^6$ Jurkat cells at 4 °C in Tris-buffered saline in the presence of 1 mM Ca^{2+} and Mg^{2+}. The bound phage were rescued after three washes with phosphate-buffered saline by adding 300 μL of K91Kan bacteria for 30 min at room temperature (*10*). The amount of bound phage was quantified by plating and counting TU. Inhibition of phage binding was studied by adding peptides at various concentrations or antibodies (10 μg/mL) to the assay together with the phage.

Cell Attachment Assays. Microtiter wells were coated with vitronectin at a concentration that resulted in 50−70% of the maximum cell attachment (usually 5 μg/mL). Inhibition of cell attachment mediated by the $\alpha_v\beta_3$ integrin was tested with MDA-MB-435 human breast carcinoma cells (2.5×10^4 cells per well) attached to microtiter wells coated with vitronectin. The peptides were added to the wells at various concentrations, and the degree of cell attachment was quantified by staining the cells with crystal violet (*15*).

NMR Spectroscopy. NMR spectra were acquired with a Varian UNITY-plus 500 MHz spectrometer that was equipped with a 3 mm triple resonance probe and a single-axis pulse-field-gradient accessory along the *z*-axis. The peptides were soluble in water only at pH ≥7.5. At the high pH, the amide protons are not observable due to fast amide proton to solvent exchange. Therefore, experiments were carried out at 20 °C (unless indicated otherwise) in a dimethyl sulfoxide solution. The total volume in a 3 mm NMR tube is 220 μL. Initial two-dimensional homonuclear experiments (NOESY, TOCSY, ROESY, and 2DQF-COSY) were carried out on samples of RGD-A and RGD-B at a sample concentration of 5 mM in DMSO-d_6. To carry out the natural abundance ^{13}C experiment, we increased the concentration to 11 mM. The peptides were extremely soluble in DMSO-d_6. Homonuclear two-dimensional NMR NOESY (τ_{mix} = 75, 150, 300, and 400 ms), TOCSY (τ_{mix} = 50 ms), and DQF-COSY (acquired at 20, 25, 30, 35, and 40 °C to determine the temperature coefficients of amide protons) spectra were acquired. The transmitter carrier was placed on the water resonance, and that resonance was saturated by a low-power radio frequency pulse during the relaxation delay. A band-selected homonuclear-decoupled NOESY experiment (BASHD-NOESY, τ_{mix} = 300 ms) was also acquired with spectral widths in the ω_1 and ω_2 dimensions of 8000 and 600 Hz, respectively. This experiment was designed for high digital resolution (*16*) in the second dimension along the α proton region so more NOEs could be obtained in that usually crowded spectral area. The band-selective π pulse is a Gaussian cascade Q3 pulse with phase modulation to shift its inversion center to the center of the H^α resonances. Gradient heteronuclear multiple-quantum experiments, ^{13}C-HMQC, were performed to assign C^α and C^β chemical shifts. The carbon carrier frequency was kept at 56 ppm with a spectral width of 6000 Hz in the carbon dimension. ^1H NMR and ^{13}C NMR chemical shifts are reported downfield from external TSP-d_4 and DSS, respectively. The States−TPPI method was used for quadrature detection in all indirectly detected dimensions. NMR data were processed and analyzed using Felix98 software (MSI, San Diego, CA) on an SGI Indigo workstation.

Experimental Constraints. Distance constraints were extracted from two-dimensional NOESY spectra, with mixing times of 75 and 150 ms, and from two-dimensional BASHD-NOESY spectra. NOE cross-peaks with strong intensities were classified to correspond with interproton distances of 1.8−2.7 Å, where the lower bound, 1.8 Å, is the closest possible interproton distance consistent with van der Waals repulsion. NOE cross-peaks with medium, weak, and very weak (the latter generating a single contour in plots) intensities in 150 ms mixing time spectra were classified into interproton distances of 1.8−3.3, 1.8−5.0, and 3.0−6.0 Å, respectively. Pseudoatom corrections were used to modify the upper bound distance constraints for NOEs involving methyl and methylene groups (*17*). $^3J_{HN\alpha}$ coupling constants were obtained from DQF-COSY spectra and used to calculate the backbone dihedral angle ϕ based on the equation

$$^3J_{HN\alpha} = 6.98 \cos^2 \theta - 1.38 \cos \theta + 1.72$$

where $\theta = |\phi - 60°|$ (*18*). The χ_1 dihedral angles were defined on the basis of the NOE intensities between

$H^N-H^{\beta 1}$ and $H^N-H^{\beta 2}$ in comparison with the NOE intensities between $H^\alpha-H^{\beta 1}$ and $H^\alpha-H^{\beta 2}$ (*19*), which is for the same residue; if NOE intensities of $H^N-H^{\beta 1} > H^N-H^{\beta 2}$ and $H^\alpha-H^{\beta 1} < H^\alpha-H^{\beta 2}$, χ_1 could be defined as $60 \pm 30°$.

Structure Calculations. A full conformational space search included generating 100 starting structures for each peptide, using distance geometry based on NMR-derived constraints. Each of the subembedded coordinates was regularized with template fitting, correct enantiomer testing, high-temperature dynamics (2000 K), and simulated annealing (*20*, *21*). Structures with relatively low empirical energies and low distance and dihedral angle constraint violations were selected for further refinement with additional constraint data from the chemical shifts of C^α, C^β, and H^α as well as the coupling constants $^3J_{HN\alpha}$. Data from overlapped or significantly line broadened DQF-COSY cross-peaks were not used. A hydrogen bond constraint was not used in the calculations. All calculations of distance geometry and restrained molecular dynamics were performed on an SGI Indigo workstation with the program X-PLOR-3.851 (*20*).

RESULTS

Integrin Specificity of RGD-4C Phage Binding to Cells. The RGD-4C phage was originally identified by phage library screening on the $\alpha_v\beta_5$ integrin and shown to bind avidly to this integrin and to $\alpha_v\beta_3$. We chose Jurkat cells to further analyze the integrin specificity of this phage, because these cells express a variety of integrins. The level of binding of RGD-4C phage to the Jurkat cells was about 400-fold higher than that of control phage expressing an unrelated insert or no insert at all. Binding was inhibited by 90% in the presence of the function-blocking anti-$\alpha_v\beta_3$ antibody (Figure 1). Function-blocking anti-β1 had no significant effect. We also tested anti-$\alpha M\beta$2 and anti-α4 antibodies, because the $\alpha M\beta$2 integrin binds to fibrinogen in an RGD-dependent manner (*22*) and $\alpha_4\beta_1$ binds to a motif in fibronectin that is distinct from, but related to, RGD (*23*; see ref *2* for review). No inhibition was seen (Figure 1). The RGD-4C peptides inhibited the binding of the RGD-4C phage to the Jurkat cells; the RGD-A isomer was 18 times more potent than the RGD-B isomer.

Integrin Specificity of RGD-4C Peptide Isomers in Cell Attachment. RGD-A potently inhibited the attachment of MDA-MB-435 cells to vitronectin, whereas RGD-B was about 6-fold less potent in this assay (Figure 2). Anti-integrin antibody inhibition experiments showed that vitronectin attachment of these cells is mediated by the $\alpha_v\beta_3$ integrin (data not shown). Thus, the RGD-A isomer primarily accounts for the previously noted binding of RGD-4C to the α_v integrins (*10*). In contrast, RGD-A and RGD-B were both weak inhibitors of $\alpha_5\beta_1$-mediated cell attachment to fibronectin (data not shown).

Resonance Assignments and Confirmation of Disulfide Bridge Connectivity. Most proton and carbon chemical shifts were assigned unambiguously for RGD-A and RGD-B. The NMR experiments were carried out at 20 °C to overcome cross-peak overlap in the ^1H dimension. However, for RGD-A, the amide proton resonances as well as the α proton resonances for residues Cys2 and Cys3 remained overlapped at different temperatures with very slight dispersion. To assign one of the overlapped cysteine resonances and to prove

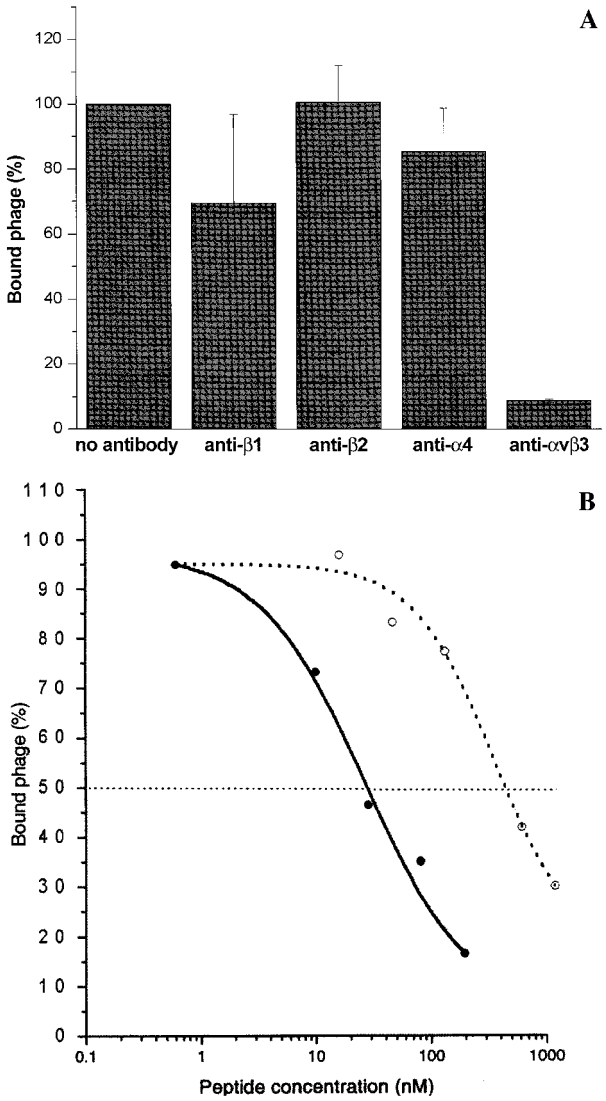

FIGURE 1: Binding of RGD-4C phage to Jurkat cells. Phage displaying the peptide were incubated with Jurkat cells in the presence and absence of anti-integrin antibodies (A) and peptides (B), and the bound phage was quantified. The phage binding was normalized relative to when no antibodies or peptides were added. The results represent means and standard deviations from two experiments made in triplicate: (—) RGD-A and (- - -) RGD-B.

their superimposed chemical shifts, we confirmed connectivities through the NOEs observed from the amide proton resonances to the side chains of their preceding residues. Amide proton resonances for residues Cys2 and A1 are also indistinguishable in RGD-B (chemical shift assignments available as Supporting Information in Tables I−III). The quality of the NOESY spectra as well as the BASHD-NOESY data acquired to increase the digital resolution in the relatively crowded H^N-H^α fingerprint region was acceptable. The BASHD-NOESY data allowed further confirmation of the assignments, which can be easily observed (Figures 1 and 2 in the Supporting Information). Natural abundance gradient ^{13}C HMQC spectra were obtained for each peptide. The high signal-to-noise quality of these spectra allowed unambiguous assignments for the $^{13}C\alpha$ and $^{13}C\beta$ resonances (Figures 3 and 4 in the Supporting Information).

The NOE patterns for the two isomers were unique and easily distinguishable. Although the disulfide bridge connectivities for RGD-A could not be confirmed directly due

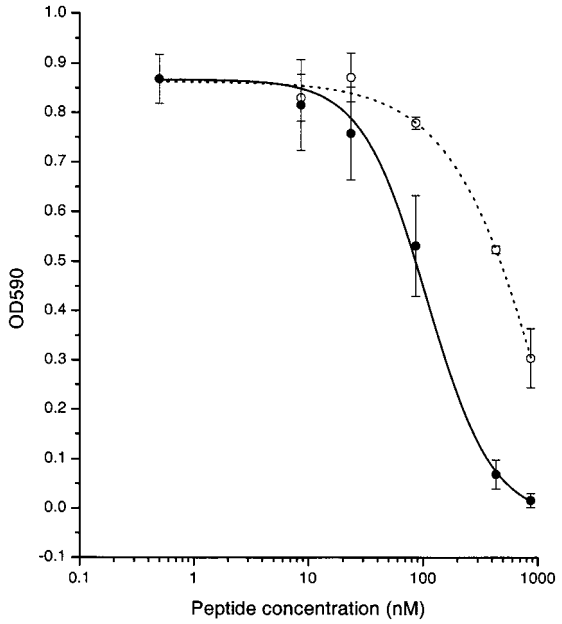

FIGURE 2: Inhibition of cell attachment by the RGD-4C peptides. Microtiter wells were coated with vitronectin, MDA-MB-435 breast carcinoma cells were added to the wells together with the indicated amounts of the RGD-A (—) and RGD-B (- - -) peptides, and cell attachment was assessed. The results represent means of measurements made in triplicate. The background has been subtracted.

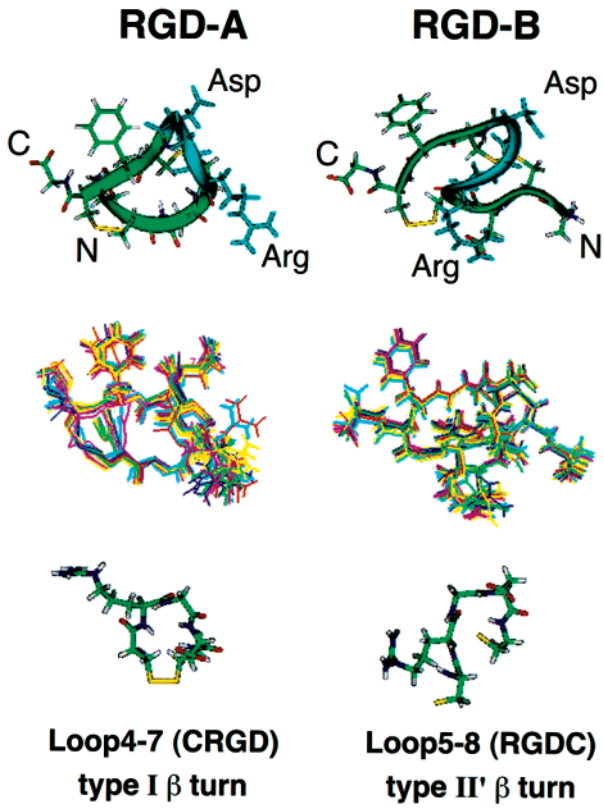

FIGURE 3: Ribbon representations of the NMR structures of the RGD-A and RGD-B peptides (top panel). The superimposed solution structures are the ensembles of 19 structures for each peptide. For RGD-A, the pairwise standard deviations (rmsds) of the ensemble are 0.491 ± 0.152 Å for backbone atoms and 1.281 ± 0.403 Å for all non-hydrogen atoms. The total energy, including covalent and nonbonded geometry, is 36.3 ± 4.2 kcal mol^{-1}. There are no NOE violations out of 93 distance constraints used in calculations of >0.3 Å, and no violations for the dihedral angles of >5°. For RGD-B, the pairwise rmsds of the ensemble of 19 structures are 0.360 ± 0.165 Å for backbone atoms and 1.045 ± 0.244 Å for all non-hydrogen atoms. The total energy, including covalent and nonbonded geometry, is 66.9 ± 2.6 kcal mol^{-1}. There are no NOE violations out of 131 used in calculations of >0.3 Å and no violations for the dihedral angles of >5°. More detailed statistical data are available as Supporting Information. As determined from NMR data, the C_2RGD segment, a distorted type I β-turn for the RGD-A peptide, and the $RGDC_3$ segment, a type II′ β-turn for RGD-B the peptide, are shown.

to the overlap in Cys2 and Cys3, all four Cys residues in RGD-B were well-resolved. We observed NOEs between Cys1 and Cys3 in RGD-B, thus confirming its disulfide bridge connectivity. For RGD-A, the disulfide bridge connectivity was identified by analyzing of the NOEs to contiguous side chains.

Structures of RGD-A and RGD-B. The conformations of the two isomers, and especially the loop containing the RGD residues, were first analyzed with respect to hydrogen bonding. Most temperature coefficients for RGD-A were above −4 ppb K^{-1} with one exception, −2.5 ppb K^{-1} (Table III in the Supporting Information), indicating that all of the amide protons were partially or fully solvent exposed. In RGD-B, temperature coefficients of less than −2 ppb K^{-1} were observed for two residues: Arg (−0.2 ppb K^{-1}) and Cys3 (−1.5 ppb K^{-1}) in the $RGDC_3$ segment. The existence of a hydrogen bond in the $RGDC_3$ segment could not be confirmed, because to form a proper hydrogen bond between the amide proton of Cys3 and the carbonyl group of Arg, the amide proton of Arg would need to be rotated and exposed to solvent. A low temperature coefficient was measured experimentally for the Arg and Cys3 amide protons. No hydrogen bonds were imposed from these two amide protons to other surrounding electron acceptors to avoid bias of the initial structure calculations. The temperature coefficient is taken solely as an indication of partial protection of the Arg and Cys3 amide protons.

The numbers of experimental constraints available for these 11 residue peptides were considered adequate, and the initial decision not to impose hydrogen bonding for RGD-B was based on the sufficient data that were available. For RGD-A, 97 distance constraints and 9 dihedral angle constraints were used in the structure calculations. For RGD-B, a total of 131 distance constraints and 11 dihedral angle constraints were considered. Further refinement of the structures using all the ^1H and ^{13}C chemical shifts, as well as ^3J values, resulted in the reported structures. These structures have very low energies and low numbers of violations (see the Figure 3 legend). Analysis of the final structures for RGD-B shows that the amide protons for residues Arg and Cys3 are indeed buried within the structure. This result agrees well with the observed low temperature coefficient.

The side chain from the Phe residue in RGD-A was not restrained initially. We note that a hydrophobic moiety in this position (adjacent to the RGD fragment) is always selected by the initial phage display experiments (*10*). The calculated structures allowed the aromatic Phe ring to flip between two positions. Careful measurements of the χ_1 angle (see Materials and Methods), and inclusion of imposed 60° χ_1 constraints in the later calculations led to the structures for RGD-A shown in Figure 4. The superimposed final ensembles of 19 acceptable structures for each peptide are

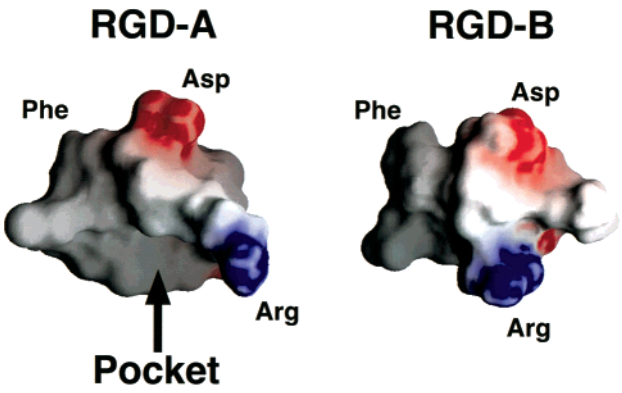

FIGURE 4: GRASP (*37*) representations of the molecular surfaces of RGD-A and RGD-B, color coded by electrostatic potential. Blue and red correspond to positive (Arg) and negative (Asp) potential, respectively. The Phe hydrophobic ring for each isomer is marked as well as a deep pocket in RGD-A.

shown in Figure 4, and the ribbon representations highlight the backbone traces of each structure. The two isomers present entirely different structures. Also shown in Figure 4 are the specific RGD loops for RGD-A and RGD-B. These loops exhibit different β-turn conformations for each isomer: a type I β-turn for the C_2RGD segment in RGD-A and a type II′ β-turn for the RGDC_3 segment in RGD-B.

To satisfy the Cys2−Cys3 disulfide linkage in RGD-A, the carbonyl moiety of the Cys2 residue is pushed away from the interior of the loop, which leads to a distorted type I β-turn. The deviations for the ϕ_2 and ψ_2 dihedral angles from the standard type I β-turn are ~90° and ~50°, respectively, and therefore, no hydrogen bonding could form in this β-turn. Dihedral angles for other residues in the turn satisfy standard type I β-turn values within ±30°, and the distance from residue C^{α}_i to residue C^{α}_{i+3} residues in the turn is 5.0 Å.

The type II′ β-turn in RGD-B is also distorted at the ϕ_2. As mentioned, the amide protons for Arg and Cys3 are both partially protected as measured by the low-temperature coefficient data. Besides the ϕ_2 distortion, the rest of the β-turn exhibits typical type II′ characteristics with ϕ and ψ dihedral angle deviations within ±30°. The distance from residue C^{α}_i to residue C^{α}_{i+3} in the turn is 6.1 Å (*24*−*26*).

The statistics of the calculated structures based on our NMR data are given in the legend of Figure 3 and are also available in the Supporting Information (Tables IV and V). The obtained structures satisfy all commonly accepted criteria for structural calculations as specified in the literature. In addition, the PROCHECK-NMR program (*27*) was used to examine the structure validations in terms of the dihedral angles. More than 75 and 98% of the residues were found in the most favored and additional allowed regions for RGD-A and RGD-B, respectively. No residues populate the disallowed regions in either of the two isomers that have been studied.

DISCUSSION

The results reported here show that RGD peptides with the same primary sequence can differ in their integrin binding specificity, depending on the position of their disulfide bonds. The solution structures show that the presentation of the RGD motif in the two isomers is quite different, explaining their divergent integrin binding activities. These structures may be helpful in the design of selective inhibitors for integrins.

The alternate disulfide bridge connectivities in the two isomers produce different backbone trajectories, placing the RGD motif in different orientations (Figures 3 and 4). The Phe residue and the disulfide bridges are used as guides in comparing the two isomers. We found that the orientation of the Asp residue is similar in the two isomers, but the orientation of the Arg residue is quite different. In RGD-A, the Arg is closer to the Asp residue, whereas these two residues are far apart from each other in RGD-B. The distance between the C^{β} atoms of Arg and Asp in the two isomers is 6.3 and 8.6 Å, respectively. The relative orientation of the Arg guanidinium ion and of the carboxyl moiety from Asp in the RGD motif may dictate selectivity toward different integrins (*28*). Furthermore, the position of the RGD motif relative to the flanking hydrophobic ring from Phe is also influenced by the disulfide bridge patterns.

In both isomers, the RGD sequence forms a well-defined β-turn conformation, although no hydrogen bond is ascertained. RGD-A displays a modified type I β-turn in the C_2-RGD segment, with the carbonyl group from Cys2 exposed to the solvent. This distortion may make the carbonyl group available for hydrogen bonding to the integrin, as previously suggested (*29*).

The RGD-B isomer forms a type II′ β-turn in the RGDC_3 segment. The type II′ β-turn with G and D in positions 2 and 3 of the turn, respectively, has been observed in RGD proteins (*30*, *31*). In our studies, the type II′ β-turn is distorted at the carbonyl group of the Arg. The RGD-B structure shows the amide protons of Arg and Cys3 not exposed to solvent, and this result agrees with our experimental temperature coefficient data. The existence of a hydrogen bond is not essential for a stable β-turn conformation. Examples exist in the literature of non-hydrogen-bonded β-turns in protein structure that are not detrimental to the structural and functional integrity of these turns (*32*).

It has been suggested that induction of a type II′ β-turn to a type I β-turn may modulate receptor specificity and result in side chain orientations that are conducive to preferred interaction with the $\alpha_v\beta_3$ integrin (*28*). A distance of less than 6.7 Å between C_β of Arg and C_β of Asp seemed to be especially favorable for $\alpha_v\beta_3$ binding. Our RGD-A isomer results agree with this suggestion. In RGD-A and RGD-B, the preponderance of a type I β-turn is dictated by the choice of disulfide bridge partners in the peptide.

Another major structural difference observed between RGD-A and RGD-B is the presence of a pocket formed by the hydrophobic residue Phe and a part of the N-terminus in RGD-A; this pocket is not observed in RGD-B (Figure 4). Possibly, the hydrophobic residue participates in interactions with a hydrophobic patch within the receptor. Such secondary interactions may aid in creating the specificity for the $\alpha_v\beta_3$ and $\alpha_v\beta_5$ integrins. Hydrophobic residues flanking the RGD motif on the carboxyl side of the RGD motif have been shown to be preponderant in phage display selection for biologically active, highly inhibitory sequences (*10*) and can enhance the binding activity of chemically synthesized cyclic RGD peptides (*33*, *34*).

Though the side chains are presumed free to move in solution, the doubly bridged RGD-B isomer separates the RGD motif into a subregion with the negatively charged Asp

residue adjacent to a hydrophobic amino acid and spatially independent of the Arg moiety. This presentation of the Asp residue may favor selective binding of a peptide to integrins, reminiscent of Asp40 in the QIDSPL sequence of V-CAM-1 that is critical to $\alpha_4\beta_1$ binding (*23*) and the ICAM-1 Glu34 residue that mediates $\alpha_L\beta_2$ binding of ICAM-1 (*35*). However, we have been unable to show conclusively that RGD-B binds preferentially to either α_4 or β_2 in the systems we have tested.

RGD-4C provides a particularly clear demonstration that the presentation of the RGD motif in peptides and proteins is critical to integrin recognition. Previous results have shown that cyclization of an RGD-containing peptide, and assigning appropriate amino acid residues to the positions flanking the RGD, can increase the integrin binding potency of a peptide and enhance its selectivity for a given integrin (*2*, *3*). The RGD-A peptide is a highly potent and selective ligand for the $\alpha_v\beta_3$ and $\alpha_v\beta_5$ integrins ($K_d \sim 100$ nM; *10*). The unique feature of RGD-A and RGD-B peptides is that the two cyclic peptides are created from the same primary sequence and yet differ in their integrin binding properties.

The NMR studies presented here yield the structures of the free peptides in solution, and ideally, the bound structures should be elucidated with heteronuclear filtered methods. The NMR structures of these peptides represent highly populated conformations within the ensemble of accessible conformations in solution. These highly restricted peptides provide insights into the possible factors needed for stereospecific inhibition of different members of the integrin family. The structures we report should be useful for designing inhibitors and ligand mimics for individual integrins. The importance of the $\alpha_v\beta_3$ and $\alpha_v\beta_5$ integrins in angiogenesis (*7*, *8*) and osteoporosis (*36*) makes these structures particularly relevant.

ACKNOWLEDGMENT

We thank Johan Rung and Drs. Wadih Arap, Erkki Koivunen, and Renata Pasqualini for their help at the early stages of this work.

SUPPORTING INFORMATION AVAILABLE

Chemical shifts, coupling constants, temperature coefficients, structural statistics, and spectra of RGD-A and RGD-B. This material is available free of charge via the Internet at http://pubs.acs.org.

REFERENCES

1. Hynes, R. O. (1992) *Cell 69*, 11−25.
2. Ruoslahti, E. (1996) *Annu. Rev. Cell Dev. Biol. 12*, 697−715.
3. Pierschbacher, M. D., and Ruoslahti, E. (1987) *J. Biol. Chem. 262*, 17294−17298.
4. Brooks, P. C., Stromblad, S., Klemle, R., Visscher, D., Sarkar, F. H., and Cheresh, D. A. (1995) *J. Clin. Invest. 96*, 1815−1822.
5. Hammes, H.-P., Brownlee, M., Joonczyk, A., Sutter, A., and Preissner, K. T. (1996) *Nat. Med. 2*, 529−533.
6. Yamamoto, M., Fisher, J. E., Gentile, M., Seedor, J. G., Leu, C. T., Rodan, S. B., and Rodan, G. A. (1998) *Endocrinology 139*, 1411−1419.
7. Arap, W., Pasqualini, R., and Ruoslahti, E. (1998) *Science 279*, 377−380.
8. Brooks, P. C., Montgomery, A. M., Rosenfeld, M., Reinsfeld, R. A., Hu, T., Klier, G., and Cheresh, D. A. (1994) *Cell 79*, 1157−1164.
9. Friedlander, M., Brooks, P. C., Sharffer, R. W., Kincaid, C. M., Varner, J. A., and Cheresh, D. A. (1995) *Science 270*, 1500−1502.
10. Koivunen, E., Wang, B., and Ruoslahti, E. (1995) *Bio/Technology 13*, 265−270.
11. Pasqualini, R., Koivunen, E., and Ruoslahti, E. (1997) *Nat. Biotechnol. 15*, 542−546.
12. Ellerby, H. M., Arap, W., Ellerby, L. M., Kain, R., Andrusiak, R., Rio, G. D., Krajewski, S., Lombardo, C. R., Rao, R., Ruoslahti, E., Bredesen, D. E., and Pasqualini, R. (1999) *Nat. Med. 5*, 1032−1038.
13. Wickham, T. J., Carrion, M. E., and Kovesdt, I. (1995) *Gene Ther. 2*, 750−756.
14. Dmitriev, I., Krasnykh, V., Miller, C. R., Wang, M., Kashentseva, E., Mikheeva, G., Belousova, N., and Curiel, D. T. (1998) *J. Virol. 72*, 9706−9713.
15. Pasqualini, R., Koivunen, E., and Ruoslahti, E. (1995) *J. Cell Biol. 130*, 1189−1196.
16. Krishnamurthy, V. V. (1997) *Magn. Reson. Chem. 35*, 9−12.
17. Wüthrich, K., Billeter, M., and Braun, W. (1983) *J. Mol. Biol. 169*, 949−961.
18. Wang, A. C., and Bax, A. (1996) *J. Am. Chem. Soc. 118*, 2483−2494.
19. Kessler, H., and Seip, S. (1994) NMR of peptides, in *Two-dimensional NMR spectroscopy: Applications for chemists and biochemists* (Croasmun, W. R., and Carlson, R. M. K., Eds.) 2nd ed., pp 642−643, VCH Publishers, New York.
20. Brünger, A. T. (1993) *X-PLOR Version 3.1: A system for X-ray crystallography and NMR*, Yale University Press, New Haven, CT.
21. Nilges, M., Clore, G. M., and Gronenborn, A. M. (1988) *FEBS Lett. 229*, 317−324.
22. Wright, S. D., Weitz, J. I., Huang, A. J., Leven, S. M., Silverstein, S. C., and Loike, J. D. (1988) *Proc. Natl. Acad. Sci. U.S.A. 85*, 7734−7738.
23. Wang, J. H., Pepinsky, R. B., Stehle, T., Liu, J. H., Karpusas, M., Browning, B., and Osborn, L. (1995) *Proc. Natl. Acad. Sci. U.S.A. 92*, 5714−5718.
24. Chou, K.-C., and Blinn, J. R. (1997) *J. Protein Chem. 16*, 575−595.
25. Hutchison, E. G., and Thornton, J. M. (1994) *Protein Sci. 3*, 2207−2216.
26. Wilmot, C. M., and Thornton, J. M. (1988) *J. Mol. Biol. 203*, 221−232.
27. Laskowski, R. A., Rullmann, J. A., MacArthur, M. W., Kaptein, R., and Thornton, J. M. (1996) *J. Biomol. NMR 8*, 477−486.
28. Bach, A. C., Espina, J. R., Jackson, S. A., Stouten, P. F. W., Duke, J. L., Mousa, S. A., and DeGrado, W. F. (1996) *J. Am. Chem. Soc. 118*, 293−294.
29. Haubner, R., Gratias, R., Diefenbach, B., Goodman, S. L., Jonczyk, A., and Kessler, H. (1996) *J. Am. Chem. Soc. 118*, 7461−7472.
30. Dyson, J. H., Bolinger, L., Feher, V. A., Osterhout, J. J., Jr., Yao, J., and Wright, P. (1998) *Eur. J. Biochem. 255*, 462−471.
31. Krezel, A. M., Wagner, G., Seymourulmer, J., and Lazarus, R. A. (1994) *Science 264*, 1944−1947.
32. Leahy, D. J., Aukhil, I., and Erickson, H. P. (1996) *Cell 84*, 155−164.
33. Gurrath, M., Muller, G., Kessler, H., Aumailley, M., and Timpl, R. (1992) *Eur. J. Biochem. 210*, 911−921.
34. Jois, S. D., Tambunan, U. S., Chakrabarti, S., and Siahaan, T. J. (1996) *J. Biomol. Struct. Dyn. 14*, 1−11.
35. Casasnovas, J. M., Stehle, T., Liu, J. H., Wang, J. H., and Springer, T. A. (1998) *Proc. Natl. Acad. Sci. U.S.A. 95*, 4134−4139.
36. Rodan, S. B., and Rodan, G. A. (1997) *J. Endocrinol. 154* (Suppl. S), 47−56.
37. Nicholls, A., Sharp, K., and Honing, B. (1991) *Proteins: Struct., Funct., Genet. 11*, 281−296.

BI002101F